Interfacial Phenomena in Polymer Blends: A Self-Consistent Brownian Dynamics Study

Bharadwaj Narayanan, Victor A. Pryamitsyn, and Venkat Ganesan*

Department of Chemical Engineering, University of Texas at Austin, Austin, Texas 78712

Received May 21, 2004; Revised Manuscript Received October 3, 2004

ABSTRACT: We apply a recently proposed multiscale simulation approach to study the dynamical properties of polymer blend interfaces. We use this approach to study the influence of the bulk rheological properties of the polymer blend components upon the slip at unentangled polymer interfaces. Our numerical results agree quite well with the predictions from scaling approaches and phenomenological theories. Moreover, these results also provide a microscopic explanation of the negatively deviating viscosities of polymer blends. We also present results elucidating the slip suppressing influence of block copolymer compatibilizers. Our results suggest that even trace fractions of compatibilizers can suppress slip at polymer interfaces. We study the influences of the molecular weight of the block copolymer and the coverage of block copolymers upon the dynamical properties of polymer blend interfaces, and we suggest some effects that might account for the effect of compatibilizers in the suppression of coalescence during polymer blending.

I. Introduction

Properties (mechanical, optical, and electrical) of many multicomponent polymeric systems, which include polymer blends, polymer solutions, and block copolymer melts, depend on their morphological characteristics.[1−3] In recent years, flow processing of multicomponent polymeric materials has emerged as an inexpensive and versatile route to control their microstructural characteristics and enhance their properties.[4−8] For instance, flow-based melt blending of two or more immiscible polymeric materials has widely been used as a route to develop polymeric materials possessing a combination of desired properties.[1] An important aspect that confronts such applications is the effect of the flow field on the morphological characteristics of the polymeric material, i.e., interplay between structure and rheology. Consequently, developing predictive means to address this question is expected to have significant practical implications.

Intriguing experimental results have been reported in the literature that document the profound effects arising from the interplay between flow and thermodynamical characteristics. Scattering experiments by Higgins and co-workers[9−11] have demonstrated that the phase curve of binary polymer blends could be shifted by more than 10% due to the application of shear. Bates and co-workers[12] have reported shear influenced order−disorder transition shifts in symmetric block copolymers. More recently, lamellae-forming triblock and pentablock copolymers have exhibited shear-induced disordering and shift in lamellar orientation (Vigild et al.[8]) Despite the technological implications of such phenomena, predicting such interplay between rheology and phase behavior of such systems remains an outstanding theoretical challenge.

Traditional kinetic-theory-based molecular models, which have been used with success to study the dynamics of homogeneous polymer solutions and melts,[13,14] do not prove directly applicable to such structured polymeric systems, especially under strong flow fields. Note that such materials are inherently inhomogeneous, and in many cases the inhomogeneity in the system (characterizing the inherent structure of the underlying multicomponent system) is on the scale of molecules themselves. A drawback of traditional molecular approaches is that they tend to focus on the conformational dynamics of noninteracting (except possibly hydrodynamically) macromolecules. On the other hand, modeling phase separating and self-assembled systems requires one to account for the interaction between polymers to accommodate (in a thermodynamically consistent manner) the resulting compositional inhomogeneity.[13,14]

Recently, many seminal advances have occurred in the context of modeling the thermodynamical and dynamical properties of polymeric materials. On one hand, polymer self-consistent-field theories have been cast into attractive numerical approaches that can enable the prediction of the thermodynamics and self-assembly characteristics of a variety of multicomponent polymers. These approaches has been used with with great success to predict the equilibrium thermodynamical features of multiblock copolymers,[15−17] blends of block copolymers with homopolymers,[18] thin films of polymers,[19] etc. On the other hand, innovative coarse-grained simulation models of polymers have been developed to address the rheological characteristics of polymers resulting from fast flows, entanglements, hydrodynamical interactions, etc.[20−23] The latter advances have allowed one to predict, with quantitative accuracy, the dynamical and rheological characteristics of a variety of polymers such as homopolymers,[21−23] star polymers,[23] DNA,[24] etc., for different flow situations.

With the above-mentioned advances, a significant surge of interest has arisen to combine the thermodynamic and dynamic ideas to model the dynamical properties of inhomogeneous multicomponent polymeric materials. Pioneering approaches by Fraaije[25,26] and by Doi, Milner, and Fredrickson[27] proposed mesoscale models that include phenomenological dynamics for slow variables like density and stress fields that approxi-

* Author for correspondence: Alfred P. Sloan Fellow; e-mail venkat@che.utexas.edu.

10.1021/ma048986a CCC: $27.50
Published on Web 11/20/2004

mately accounted for the inhomogeneity-induced changes in chain conformations and their coupling to the externally applied flow fields. While such assumptions are reasonable in capturing slow dynamical phenomena and/or weak deviations from equilibrium, their utility becomes limited in modeling strongly nonequilibrium phenomena, such as slip at the interface of polymer blends,[31,32] shear-induced orientations of multiblock copolymers,[33] role of block copolymer compatibilizers in modifying the dynamics of polymer blends,[34,35] etc. More recently, Kawakatsu and co-workers[28] proposed a powerful new approach which removes some of the assumptions underlying earlier theories and combines polymer self-consistent-field theory with the reptational dynamics arising due to entanglements. The latter method has been used successfully to model the fast flow dynamics and the molecular conformational changes occurring in the shear of entangled polymer brushes. Schnidman and co-workers have also been developing a dynamical version of the self-consistent-field theory which allows for a versatile simulation of the dynamical properties of multicomponent polymeric materials.[29]

In an earlier preliminary article,[30] we proposed a molecular simulation technique which combines single-chain-based Brownian dynamics simulations along with a field-theoretical approach to address the rheology of inhomogeneous polymeric systems. In this approach the polymer chain is still modeled at a coarse-grained level by a set of beads and springs; however, the interactions between different beads are now accounted by a potential acting on each bead. As will be explained in the next section, this method is founded upon polymer self-consistent-field theory and computes the potential in a self-consistent manner to render this mapping exact at equilibrium. One of the advantages of this framework is that it avoids the need to simulate many interacting chains, and instead noninteracting copies of single polymer chain are evolved in combination with a hybrid continuum-molecular framework. Moreover, it is also possible to incorporate this framework within alternate single-chain Brownian dynamics simulation approaches to capture (approximately) the effects arising from entanglements,[21,23] hydrodynamical interactions,[20,24] etc.

In this article, we apply our approach to study two closely related phenomena pertaining to interfacial dynamics in polymer blends. The first corresponds to the slip effects at the interface of immiscible polymer blends, and the second corresponds to the effect of block copolymer compatibilizers in modifying such interfacial dynamical properties. In the latter case, we focus on suppression of slip at blend interface and the possible role of copolymers in suppression of coalescence of two approaching drops in simple flow. The article is presented in three parts. The first part (section II) expands upon the simulation algorithm presented earlier. The second part discusses the results obtained for equilibrium and dynamical phenomena in polymer blends. Section III deals with the equilibrium results of binary polymer blend system, and section IV focuses on the slip phenomena within the context of symmetric and asymmetric polymer blends. These results are compared with related experimental and theoretical researches. The final part of the paper is devoted to studying the role of block copolymers as compatibilizers. It focuses on suppression of slip (section VA) and suppression of coalescence (section VB) by copolymers.

II. Simulation Technique

This section presents an overview of our self-consistent Brownian dynamics (SCBD) approach to model the dynamics of inhomogeneous polymers. The approach proposed combines the idea behind Doi's dynamical mean-field theory[14] (for rodlike polymers) along with self-consistent-field theory for flexible polymers[17] to develop a method that can predictively model the dynamical characteristics of flexible inhomogeneous polymeric systems. In the following section we develop the self-consistent-field theory for a system of a binary asymmetric blend. This theory rigorously maps the equilibrium properties of the binary system of interacting polymers to a system of noninteracting polymers in an external potential $W(r)$. Later, we elaborate the details of the simulation scheme that computes $W(r)$ on the fly based on the statistics of the flexible polymers.

A. Polymer Self-Consistent-Field Theory. In this section, we construct a field theory for the system comprising of a blend of two unlike polymers denoted A and B. We consider the general case where the radii of gyration of A and B can be different. We start by modeling the polymeric molecule as a continuous Gaussian thread corresponding to the continuum limit of the bead−spring representation. In this model polymer chains are represented by continuous space curves $R_\alpha(\bar{s})$, where α indexes the different polymer chains, and $\bar{s}$ denotes an arc length variable running from 0 to N_k, where k indexes the type of species (A or B). In the field theoretic framework, the microscopic monomer densities are expressed as

$$\hat{\rho}_k = \sum_{\alpha=1}^{m_k} \int_0^{N_k} \mathrm{d}\bar{s}\ \delta(r - R_{\alpha k}(\bar{s})) \tag{1}$$

where m_k denotes the number of chains of type k. Bonded interactions in the Gaussian thread model for a binary polymer blend ($A + B$) are represented by an elastic interaction potential given by (in nondimensional units such that the arc length variable, s, runs from 0 to 1 instead of 0 to N_k, and $s = \hat{s}(N_B/N_A)$))

$$U_0[R_A,R_B] = \frac{k_\mathrm{B}T}{4R_{\mathrm{g},A}{}^2} \sum_{\alpha=1}^{m_A} \int_0^1 \mathrm{d}s \left(\frac{\mathrm{d}R_{\alpha A}(s)}{\mathrm{d}s}\right)^2 + \frac{k_\mathrm{B}T}{4R_{\mathrm{g},B}{}^2} \sum_{\alpha=1}^{m_B} \int_0^1 \mathrm{d}\hat{s} \left(\frac{\mathrm{d}R_{\alpha\beta}(\hat{s})}{\mathrm{d}\hat{s}}\right)^2 \tag{2}$$

Nonbonded intermolecular interactions are described by a standard quadratic form of microscopic monomer densities[15]

$$U_1[R_A,R_B] = \frac{k_\mathrm{B}T\chi}{\rho_0} \int \mathrm{d}r\ \hat{\rho}_A \hat{\rho}_B \tag{3}$$

where χ is the Flory parameter, ρ_0 is the total average monomer density, as $\rho_0 \equiv (m_A N_A + m_B N_B)/V$. We assume for simplicity that the monomeric volumes of the beads are identical, i.e., $v_0 = v_A = v_B \equiv 1/\rho_0$. The incompressibility constraint is imposed by a delta functional $\delta(\hat{\rho}_A + \hat{\rho}_B - \rho_0)$, restricting that the sum of the microscopic individual densities, $\hat{\rho}_A(r) + \hat{\rho}_B(r)$, be equal to the average total monomer density ρ_0.

By following the steps outlined in Fredrickson et al.,[17] we convert the above model involving conformation path

integrals of the chains into a field theory where the fundamental degrees of freedom are fluctuating chemical potential fields. In such a framework the partition function can be expressed as

$$Z = \int D[w] \int D[\pi] \exp(-H[w,\pi]) \tag{4}$$

where the Hamiltonian $H[w,\pi]$ can be expressed as

$$H[w,\pi] = \frac{-\rho_0}{\chi N_A{}^2} \int \mathrm{d}r\, w^2(r) - \frac{i\rho_0}{N_A} \int \mathrm{d}r\, \pi(r) + m_A \ln Q_A + m_B \ln Q_B \tag{5}$$

where

$$Q_i = \int DR_i \exp\left[\frac{-1}{4R_{g,i}{}^2} \int_0^1 \mathrm{d}s \left(\frac{\mathrm{d}R_i(s)}{\mathrm{d}s} \right)^2 + \int_0^1 \mathrm{d}s\, (i\pi(R_i(s)) + w(R_i(s))) \right] \quad (i = A/B) \tag{6}$$

can be interpreted as the partition functions of a single polymer (of type A/B) in a potential field. Polymer self-consistent-field theory corresponds to a saddle point approximation of the above field theory. In this framework, the saddle point values of the fields w, π are given by the solution of the following coupled equations

$$w^* = \frac{\chi\rho_0}{2}[\phi_A(r) - \phi_B(r)]; \quad \phi_A(r) + \phi_B(r) - 1 = 0 \tag{7}$$

where $\phi_k(r)$ denotes the average individual (microscopic) compositions and is defined as $\langle \hat{\rho}_k \rangle / \rho_0$, where $\langle \cdots \rangle$ represents an average over the statistics of noninteracting chains.

B. Single Chain Evolution. We extend the above theory in a *phenomenological* way to also capture the nonequilibrium behavior of phase-separated polymeric systems. For this purpose we embed the self-consistent potential field idea (which preserves the thermodynamics) into a Brownian dynamics framework which allows us to address nonequilibrium situations.[20] In this article, we consider the situation of unentangled polymer blends, and hence we use the Rouse model to describe the dynamics of these polymers. In this model, the polymer chain is modeled as a set of N beads connected linearly by $N - 1$ springs. The dynamical equation of motion for the beads are specified by the Langevin equation[14,20]

$$\zeta \left(\frac{\mathrm{d}R_\alpha^i}{\mathrm{d}t} - v(R_\alpha^i) \right) = F_\mathrm{s} + F_\mathrm{P} + F_\mathrm{R} \tag{8}$$

where R_α^i denotes the coordinate of the ith bead of the αth chain, ζ represents a phenomenological monomeric mobility coefficient (assumed to be a constant in this work), and $v(R_\alpha^i)$ denotes the velocity field at position R_α^i. In the above equation, terms on the left-hand side represents the frictional force experienced by a bead moving at a velocity $\mathrm{d}R/\mathrm{d}t$ with respect to a medium moving at a velocity $v(R)$. The right-hand side represents the other internal (and external) forces acting on the bead. This includes the following contributions: F_R is a random force mimicking the random collisions of the solvent molecules on the polymer beads, F_s is the spring force $\equiv 3k_\mathrm{B}T[R_\alpha^{i+1} - 2R_\alpha^i + R_\alpha^{i-1}]/b^2$ acting on each bead (where b denotes the Kuhn segment length), and $F_\mathrm{P} = -\nabla W(r)$ an additional component representing the external potential force acting on the polymers.

The potential field $W(r)$ incorporated into the above Rouse framework is the main new ingredient of our nonequilibrium approach and is derived from the self-consistent-field theory formulation. Explicitly, at any given instant each bead (statistical segment) is acted on by a potential given by the self-consistent-field theory as

$$W(R_\alpha^i) = \begin{cases} -\pi(r = R_\alpha^i) - w(r = R_\alpha^i), & \text{for type } A \text{ chains} \\ -\pi(r = R_\alpha^i) - w(r = R_\alpha^i), & \text{for type } B \text{ chains} \end{cases} \tag{9}$$

where α could be a chain of type A or B. (Note that π above corresponds to $i\pi$ from the previous section and accounts for the fact that self-consistent value of π field is imaginary.)

C. Potential Evolution. In the mean-field approximation, the field theory developed above reduces to a partition function of a single chain in a mean-field potential which is a function of the local compositions. We implement this approach in the above dynamical framework by simulating many copies of noninteracting discrete bead−spring chains evolving under the action of the external potential fields. At every instant, we can adopt a space fixed lattice discretization of the volume to determine the local volume fractions $\phi_k(r,t)$ by explicitly counting the number of beads of type A and B.

In principle, the above approach can be rigorously implemented for a dense enough system of chains where the instantaneous composition fields correspond to their ensemble-averaged inhomogeneous values. On the other hand, our simulations involve finite number of monomers, which leads to artificial fluctuation effects. Consequently, instead of an adiabatic evolution slaving the potential to the instantaneous volume fractions, we propose a phenomenological prescription for the evolution of the potentials such that they follow the evolutions of the composition fields and take their saddle point values at equilibrium. Explicitly, they are evolved on the discretized lattice by the following equations

$$\frac{\mathrm{d}w(r)}{\mathrm{d}t} = \Gamma_1 \left[\frac{\chi\rho_0}{2} (\phi_A(r,t) - \phi_B(r,t)) - w(r) \right] \tag{10}$$

$$\frac{\mathrm{d}\pi(r)}{\mathrm{d}t} = \Gamma_2 [\phi_A(r,t) + \phi_B(r,t) - 1] \tag{11}$$

where Γ_1 and Γ_2 are fictitious mobilities that drive the potential evolution appropriately such that the collective fields (w, π) are evolved on slower time scales than the motion of individual beads.

We emphasize that the above approach is purely phenomenological and lacks a firm basis at the molecular level. The only constraint on the above evolution is that dictated by the physical considerations which suggest that the self-consistent potentials evolve on the time scales of collective quantities such as the compositions profiles (and the stress fields encountered later). This idea is similar in spirit to the method employed earlier by Maurits and Fraaije (termed as external potential dynamics)[36] and in Fredrickson et al.[17] for potentials in the complex plane.

D. Self-Consistent Velocity Field $v(r)$ Evolution. For inhomogeneous systems, the velocity field $v(r)$ of the polymer matrix in eq 8 can, in general, be different from the macroscopically imposed velocity field. This can be attributed to the interplay between compositional inhomogeneity and molecular level dynamics. Slip at the polymer−polymer interface represents a simple example where the externally imposed field is a simple shear, whereas the resulting flow field is an inhomogeneous shear and is quite different. For our system of polymer melts, we propose a phenomenological dynamical prescription that computes the velocity field $v(r)$ self-consistently (defined on the coarse-grained lattice) such that at steady state the ensemble averaged, local gradient of stress $\nabla\cdot\Sigma = \sum_i \phi_i \nabla W_i(r)$, where $\Sigma = \langle\tau\rangle(r)$, where $\langle\tau\rangle(r)$ corresponds to the total elastic stress and $W_i(r)$ represents the potential acting on the component i. We compute the former at each lattice cell using Kramer's expression for elastic stress given by

$$\langle\tau\rangle(r) = \langle\sum_{i,\alpha}[(R_\alpha^{i+1} - R_\alpha^i)(R_\alpha^{i+1} - R_\alpha^i)]\delta(r - R_\alpha^i)\rangle/(2\Delta s)$$

where Δs denotes the discretization of the contour variable s. To ensure the above, the velocity field $v(r)$ was evolved through an iterative procedure of the form

$$\nabla^2 v_{m+1}(r) = \nabla^2 v_m(r) - \epsilon[\nabla\Sigma_m - \nabla W_m(r)] \quad (12)$$

until convergence. Here, ϵ denotes the reciprocal of a phenomenological viscosity for self-consistent velocity field evolution which is chosen so as to ensure that the collective velocity fields are evolved slower than the individual beads. The subscripted functions denote their values corresponding to the respective iterations cited. Note that such a phenomenological evolution ensures the convergence of velocity to a steady-state value such that the stress is constant throughout the system at steady state. This limits our approach in being able to capture only the steady-state behavior and misses the unsteady-state characteristics and transients.

E. Simulation Details. Our simulations for the case of a symmetric polymer blend used a simulation box of size $16 \times 8 \times 8$ (in R_g units) containing 8000 chains. Each chain was discretized into 20 beads each. The initial conditions were generated by randomly assigning the positions for all beads, while ensuring that none of the springs were excessively stretched. We quantify the length units in terms of the radius of gyration of the polymer in the blend. We also nondimensionalize our Brownian dynamics algorithm by expressing time in terms of the reciprocal of friction coefficient ζ and setting the energy scale $k_BT = 1.0$. All our simulations were performed in two dimensions with the assumption that the steady-state self-consistent potential exhibits no axial variations. However, this does not impose any constraint on the motion of the beads, and the beads were assigned positions inside a three-dimensional box and were allowed to execute Brownian motion in all three dimensions. For such a 2D simulation, we chose the lattice cell dimensions for coarse-graining as $0.25R_g$ units in x and y directions. Random initial conditions were assigned for the potentials w and π at all the lattice points.

In the nondimensionalized formulation, there are four parameters in our simulations: the Flory interaction parameter representing the repulsion between unlike monomers, χN; Γ_1 and Γ_2, the phenomenological mobilities for the evolution of $w(r)$ and $\pi(r)$ potentials; and ϵ, the parameter for velocity field evolution. In our runs we used 0.05, 0.1, and 0.0016 (in the units discussed above) for Γ_1, Γ_2, and ϵ, respectively. To ensure the validity of this method and to maintain stability, the mobility coefficient Γ_2 has to be greater than Γ_1.[17] Moreover, Γ_1, Γ_2, and ϵ must be positive. As mentioned earlier, Γ_1 and Γ_2 arise due to the finite density of monomers, and fluctuations do arise due to the fact that the number of chains per unit volume is finite. By choosing a reasonably dense system of chains per unit volume, we minimize such effects. We chose Γ_1 and Γ_2 such that the properties computed (at steady state) did not exhibit any significant variations with the parameters. The time step for the Brownian dynamics was chosen as 0.01.

We use convergence of the composition profile to monitor whether equilibrium has been achieved. In case of shear flow, both the convergence of the velocity and the composition profiles were used as criteria which signal the attainment of steady state. The convergence was assumed to be achieved when there was less than 0.5% change in the composition and velocity profiles for two consecutive block averaging performed for an interval of $125\tau_R$. The simulations were performed for a further period of $625\tau_R$ after convergence to sample all the desired quantities. Our simulations employed a shear rate $\dot\gamma\tau_R$ of 1.2. Here τ_R denotes the Rouse relaxation time of the chain. We choose a moderately high shear rate in order to reduce any fluctuations appearing in the velocity profile. Moreover, we do not study the shear rate dependence since all the quantities computed are shear rate independent in a Gaussian chain framework. The computational time for our runs took on an average around 48 h in a single 1.8 GHz processor system.

III. Equilibrium Results

Before presenting our results on the *dynamics* of polymer blends, we validate the phenomenology underlying our simulation by examining the *equilibrium* properties of a binary polymer blend system. We first consider the case of *symmetric* polymer blends where the physical properties of the two polymers, such as chain length, segment length, friction coefficient, and segmental volumes, are identical to each other. We first consider the characteristics of a segregated blend at equilibrium. Figure 1a plots the composition profile obtained from our Brownian dynamics approach for a symmetric immiscible blend where $\chi N = 6.0$. It is evident that there are two interfaces: one situated near $x = 0$ and the other near the boundary of the simulation box. The existence of the second interface is a consequence of the periodic boundary conditions imposed. We also display the equilibrium composition profiles computed from the numerical solution of the self-consistent-field theory. The latter was obtained using the real-space method of Fredrickson and Drolet[17] using the same discretization of space and chain lengths as our Brownian dynamics simulations. As is evident from the displayed results, the results of our hybrid Brownian dynamics simulation match well with the numerical results of the self-consistent-field theory.

Using our simulations, we also computed the coexistence curves for the symmetric polymer blend. The coexistence compositions of each phase were discerned by averaging the composition values at the plateau

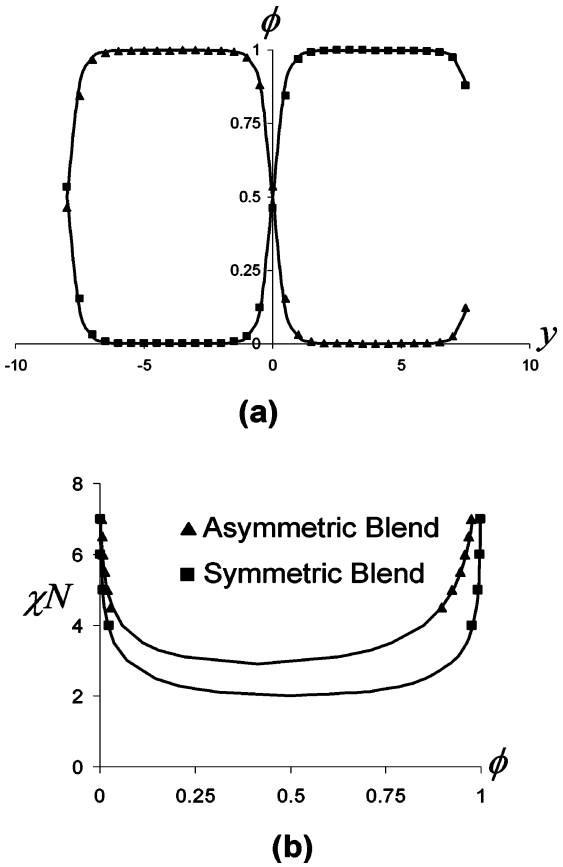

Figure 1. (a) Composition profiles of A and B components plotted as a function of spatial position for a symmetric blend with $\chi N = 7.0$. The points represent the results of our simulations, while the solid lines represent the numerical results of self-consistent-field theory. (b) Coexistence curves (binodals) for symmetric and asymmetric ($\alpha = 2.0$) blends. The points represent the results of our simulations, while the solid lines represent the numerical results of Flory−Huggins theory.

region of the composition profile and are displayed as a function of χN in Figure 1b. We were not able to get reliable coexistence compositions for shallow quenches (low χN's) because of finite size effects which precluded the existence of a plateau region in the composition profile. Shown in the same figure is the coexistence curve computed (by equating the chemical potentials and osmotic pressures in the two phases) from a Flory−Huggins form for the free energy: $-\beta F = \phi_A \ln \phi_A + \phi_B \ln \phi_B + \chi N \phi_A \phi_B$, where $\beta = 1.0/k_B T$. We note excellent agreement between coexistence compositions obtained from our hybrid algorithm and that obtained from Flory−Huggins theory. Note that, as expected for a symmetric blend, the coexistence curve is symmetric along the $\phi = 0.5$ line.

We have also studied the above equilibrium properties for the case of a polymer blend mixture where the two components differ in their chain lengths. We denote the asymmetry in the chain lengths by the parameter $\alpha = N_A/N_B$. Figure 1b displays the coexistence curve, computed as explained in the previous paragraph, for an asymmetric blend with $\alpha = 2.0$. Shown alongside in the plot is the coexistence curve computed using the Flory−Huggins theory. The asymmetry in the plot is the consequence of asymmetry in chain lengths. We again find excellent agreement between simulation and theory.

In summary, we have successfully demonstrated the applicability of our *dynamical approach* in capturing the equilibrium properties of symmetric and asymmetric blends. The results indicate a very good agreement between our simulations and the existing theories predicting equilibrium properties. While certainly our method is computationally more time-consuming and hence is not most appropriate to study equilibrium properties, nevertheless the above exercise demonstrates the applicability of the phenomenological equations (10) and (11).

IV. Slip and Shear Flow in Polymer Blends

In this section, we focus on the dynamical properties of phase separated polymer blends interfaces. Many intriguing dynamical phenomena in phase-separated polymer blends have been reported in the literature. These include shear-induced mixing, demixing and closed-loop miscibility curves, network formation in phase-separated polymer blends, slip and low mixing viscosities in polymer blends, etc. Phenomena such as shear-induced mixing, demixing, and network formation result from the effect of viscoelasticity upon thermodynamical and structural properties. On the other hand, slip and low mixing viscosities in polymer blends result from the impact of compositional inhomogeneity on the dynamical properties. While the former class of problems have had some microscopic and phenomenologically based theoretical efforts,[37,38] the latter has had comparatively fewer microscopic theories.[32] Moreover, there is still a lack of unified predictive approach that can account for both phenomena. In contrast, the approach advanced in this article can in principle account for both the effects, namely, the effect of viscoelasticity on thermodynamics and vice versa. In the present article, we study the slip phenomena in polymer blend interface, an issue which embodies the latter effect.

Anomalously low viscosities have been observed in various experimental investigations involving immiscible polymer blends,[39,40] where the blend viscosity is found to be lower than either of the pure components. These low viscosities were much lower than that of the commonly employed linear mixing rules,[41] and hence these mixtures have been termed as negatively deviating blends. A common approach to rationalize these deviations has been to suggest that the slip at the interface can lead to correspondingly low viscosities which can render the *effective viscosity* of the end component much lower than that predicted from the mixing rules.[41] While this observation has been indirect, a microscopic demonstration of this is still lacking.

When a phase-separated system of Rouse chains is subjected to a simple shear flow parallel to the interface, the bulk exhibits the Rouse viscosity $\eta_{bulk} \sim \zeta b^2 N/v_0 \sim \zeta R_g^2/v_0$. deGennes and co-workers[42] suggested that slip results from a low interfacial viscosity layer η_I sandwiched between the two bulk layers at their corresponding bulk viscosities. Further, they suggested that for unentangled interfaces η_I can be estimated as the Rouse viscosity corresponding to the number of monomers in the overlapping region of the interface. In the regime where the interfacial width a_I is large compared to the segmental length b, the latter can be estimated by balancing the enthalpic cost and the entropic gain for a loop of s segments of A entering the B-rich region to yield that the average segmental length s^* inside the interface scales as $1/\chi$. Using this expression, the interfacial viscosity can be expressed as $\eta_I \sim \zeta b^2 s^*/v_0 \sim$

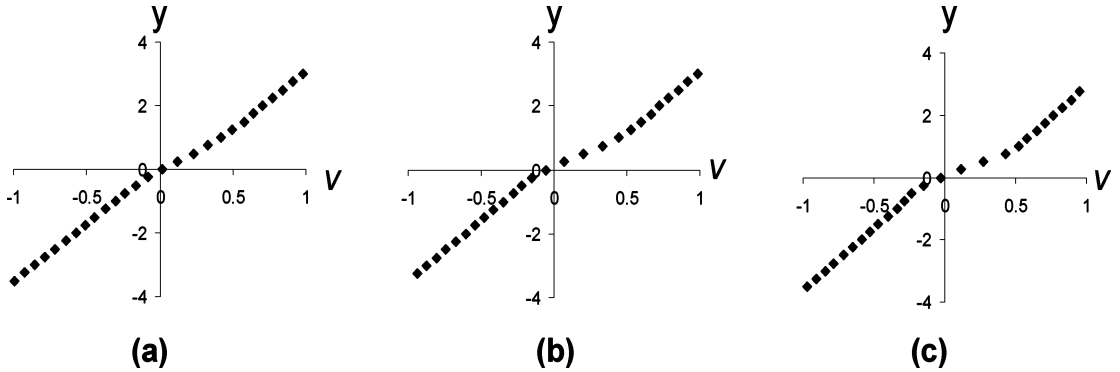

Figure 2. Steady-state velocity profiles during shear of a symmetric, segregated polymer blend: (a) $\chi N = 4.5$; (b) $\chi N = 6$; (c) $\chi N = 7.5$.

$\zeta b^2/v_0\chi$ or, in terms of interfacial thickness, a_I, as $\eta_I \sim \zeta a_I^2/v_0$. In a nutshell, the theoretical predictions suggests that (for an unentangled interface) that the interfacial slip for blends at different thermodynamic conditions are determined by the interfacial thickness, which in turn is also a thermodynamical property. The above scaling predictions have been confirmed by Fredrickson and Goveas,[32] who started from a formal Fokker−Planck equation and then used a combination of projection operators and phenomenological proposals to derive the constitutive equations for an inhomogeneous Rouse melt. More recently, Barsky and Robbins[43] used molecular dynamics simulations to probe slip phenomena in symmetric polymer blends. Their results also confirmed the scaling predictions of deGennes and theoretical results of Fredrickson. Our results, presented below, can be construed as an extension of their studies to asymmetric polymer blends.

Direct experimental measurements of slip have been complicated due to the difficulties in isolation of this specific phenomena from other dynamical phenomena in polymer blends. Recently, Zhao and Macoscko[44] provided a comprehensive investigation of the slip phenomena. They considered the extrusion of a multilayered polymer blend laminate with different numbers of layers and determined the apparent shear viscosity of the samples. Their experimental results confirmed qualitatively the predictions of the theory, while the quantitative values were somewhat lower than the theoretical predictions. Lam and co-workers[45] used rheological measurements and confocal microscopy to determine the slip at the interface between HDPE (high-density polyethylene) and polystyrene. Using confocal microscopy, they demonstrated conclusively that there is an apparent discontinuity in the velocity profile at the interface and that a smaller interfacial thickness between the blend components accentuates the slip phenomena (in qualitative agreement with the theoretical predictions).

In this study, we use our Brownian dynamics simulation approach to study slip phenomena in polymer blends. Our focus will be on validating the theoretical predictions, viz., if slip correlates directly with interfacial thickness for these systems. To this effect, we examine the slip length and the interfacial viscosities of both symmetric and asymmetric (in MWs) polymer blends. The latter involves asymmetric bulk rheological properties and hence can provide a sensitive test to the theoretical prediction that the interfacial viscosity correlates only with the thermodynamically determined interfacial thicknesses. While our Brownian dynamics simulations are on systems involving unentangled bulk components and interfaces, our results are nevertheless equally applicable to the linear rheological regime of polymer blends with entangled bulk components with unentangled interfaces. The latter situations are representative of high-MW blends encountered in practical applications, where due to the strong degree of segregation between the blend components, the interfaces are often disentangled. In such situations, the bulk viscosity is proportional to[14] $N^{3-3.4}$ while the interfacial viscosity would still correspond to the viscosity of the unentangled chains in the overlapping interfacial region as calculated in our simulations.

A. Results. In our Brownian dynamics simulation, we first equilibrate the two-layer phase-separated melt as explained in the previous section. Subsequently, a homogeneous shear field is applied on the system using a Lee−Edwards boundary condition.[46] As mentioned earlier, the applied shear rates in all simulations was kept a constant value with $\dot{\gamma}\tau_R = 1.2$. The initial velocity of all beads (at the start of shear) is specified as $\dot{\gamma} r_x$, where r_x denotes the X position of the beads and $\dot{\gamma}$ the applied shear rate. For the case of shear flow, we need to evolve the self-consistent velocities using eq 12. We compute both the self-consistent velocity field and the *nonequilibrium* composition profiles. The former quantifies slip at the interface, while the latter quantifies the role of shear upon the phase behavior. Since our simulations were performed for unentangled polymer melts, there is no coupling between the configurational statistics of the chains in the velocity and gradient directions, and consequently, shear does not have any effect upon the compositional characteristics of the blend.

We first examine the effect of the degree of incompatibility between the polymers upon the slip and dynamics in a binary polymer blend system. Figure 2a−c displays the velocity profiles of a symmetric blend for three different values of the incompatibility parameters χN corresponding to weak ($\chi N = 4.5$), intermediate ($\chi N = 6.0$), and stronger ($\chi N = 7.5$) segregations. It is evident that the self-consistent velocity profiles deviate from the homogeneous shear profile, with the deviations becoming more pronounced with an increase in the degree of incompatibility. To render these slip effects more explicit, we plot the observed shear rate as a function of position in Figure 3 for the different degrees of incompatibility. It is seen from the results that the bulk shear rates asymptote to the same value, as expected for a symmetric polymer blend system. On the other hand, the shear rates at the interface displays an increased

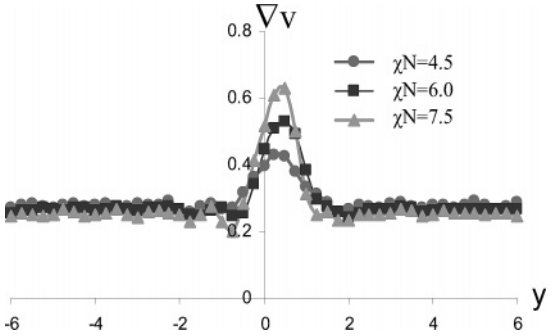

Figure 3. Velocity gradient plots as a function of the position for $\chi N = 4.5$, 6, and 7.5. Because of the periodicity of the box, the interface is shifted from $y = 0$.

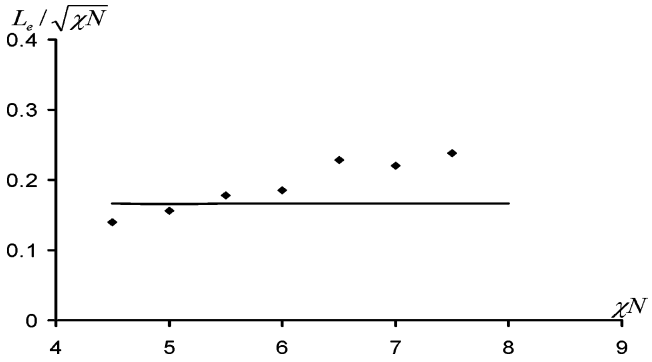

Figure 4. Extrapolation lengths (represented as the ratio $L_e/\sqrt{\chi N}$ as a function of the degree of segregation χN. The points depict the values obtained from our simulation for a symmetric blend, and the solid line represents the theoretical prediction of FG.[32]

value which becomes more pronounced with an increase in the degree of incompatibility between the polymers. The latter effect corresponds to a decrease in the effective viscosity of the interface, serving as an evidence of the slip phenomena. It is to be noted that since we have considered only Gaussian chains, shear thinning behavior is absent, and hence any lowering of viscosity is attributed to slip.

To facilitate a direct comparison with the theoretical predictions, we compute two related quantities from our results: (i) an effective slip length (or extrapolation length) L_e which quantifies the apparent viscosity of the system and (ii) the interfacial viscosity η_i. For the case of symmetric blends, it is possible to relate this slip length L_e directly to the discontinuity in the velocity at the interface Δv as $L_e \equiv \Delta v/\dot{\gamma}$, where $\dot{\gamma}$ represents the observed shear rate. On the other hand, as explained below, for asymmetric blends the L_e computed in our simulations has a more complicated dependence on the velocity profile values. Experimental,[44] theoretical,[32,47] and earlier computational studies[43] have all focused on the dependence of this slip length L_e on the degree of incompatibility between the various components. Scaling arguments[42] of deGennes suggest that the magnitude of slip should increase with an increase in the degree of incompatibility and that $L_e \sim \sqrt{\chi N}$. Fredrickson and Goveas (FG)[32] theory predicts $L_e/\sqrt{\chi N} \simeq R_g/6.0$ for symmetric polymer blends under simple shear parallel to the interface.

We computed the slip length in our simulations for symmetric polymer blends and is displayed in Figure 4 as the ratio $L_e/\sqrt{\chi N}$ as a function of χN. It is observed that consistent with the scaling arguments of deGennes

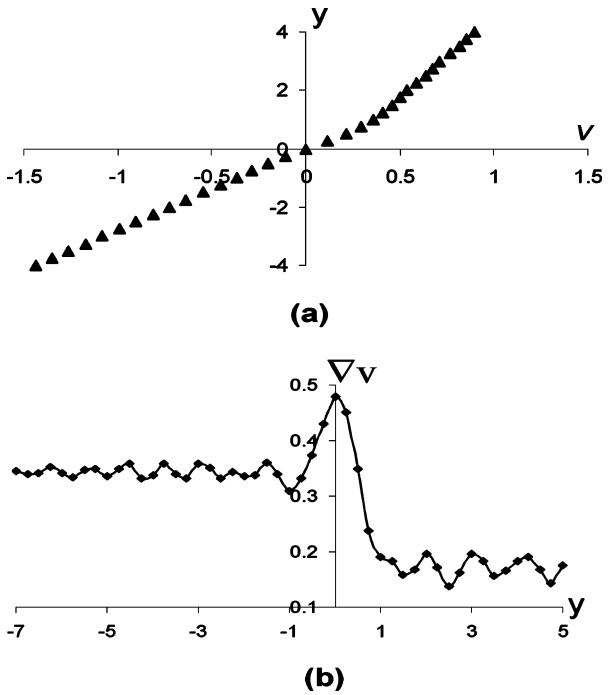

Figure 5. (a) Velocity profile. (b) Velocity gradients for an asymmetric blend with $\alpha = 2.0$ and $\chi N_A = 7.5$. In (b) the plots have been shifted such that the interface is located at $y = 0$. The noise evident in (b) is due to statistical noise in averaging and the numerical evaluation of gradients. The solid line in (b) is a guide to the eye.

that the slip length asymptotes to a constant value at strong segregation limit. Shown on the same plot is the theoretical prediction of FG.[32] It is observed that their predictions agree extremely well with our simulation results for the entire range of incompatibilities. However, unlike both the deGennes and FG predictions, our results (Figure 4) show a weak, albeit noticeable, dependence on the degree of segregation χN. These discrepancies could most likely be due to the inapplicability of the theoretical predictions for weak incompatibilities, since one of the underlying assumptions of the theory was the existence of an interface whose thickness was small compared to R_g.

To allow for a more stringent test of the theoretical predictions, we examine slip in the context of asymmetric blends. Practical situations almost always involves blend components which are asymmetric, with asymmetries resulting from unequal chain lengths (N_A, N_B), unequal chain stiffness (segmental volumes), unequal segmental friction coefficients, or a combination of one or more of these factors. In the following, as a representative example, we study the case where the asymmetry results from the asymmetries in the chain lengths. This represents a simple case where the bulk rheological properties are asymmetric, and hence the slip phenomena is expected to be impacted.

We effect numerical simulations for three different degrees of asymmetries in chain lengths between the blend components, corresponding to $\alpha \equiv N_A/N_B = 1.5$, 2, and 2.5. Figure 5a displays the numerically computed velocity profile for an asymmetric blend with $\alpha = 2.0$. The bulk phase for $x < 0$ corresponds to shorter chains (or lower viscosity polymer). Because of the asymmetry in the rheological properties of the blend, the velocity gradients in the two phases also display an asymmetry characteristic of the constancy of shear stress. To render

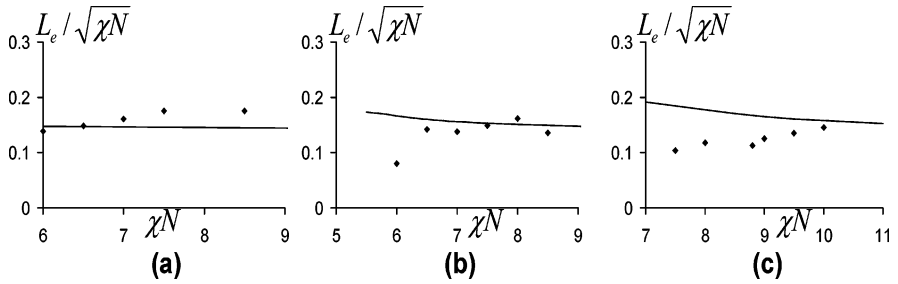

Figure 6. Slip lengths (normalized by R_g of the A chain) plotted as a function of χN_A for different degrees of asymmetries between the blend components: (a) $\alpha = 1.5$; (b) $\alpha = 2.0$; (c) $\alpha = 2.5$, where $\alpha \equiv N_A/N_B$. The points depict the values obtained from our simulation for a symmetric blend, and the solid line represents the theoretical prediction of FG.[32]

the slip at the interface more explicit, we display the shear rates in Figure 5b as computed from the velocity profile. We confirm that indeed the values of average shear rates in the bulk phases are different and asymptotic to the ratio of the bulk viscosities of the unentangled components. More interestingly, there is a jump in the observed shear rate at the interface, which confirms the lower viscosity and the manifestation of interfacial slip in these systems.

To quantify the above trends, in each of these cases we determine the apparent viscosity of the blend η_{app} by using the (constant) shear stress values and the applied shear rate. This apparent viscosity is converted to an effective slip length L_e using the following relationship:

$$L_e = L\left(\frac{\eta_{eff}}{\eta_{app}} - 1\right) \tag{13}$$

where η_{eff} represents the effective viscosity of a two-layered polymer blend in the absence of any slip effects, and L denotes the size of the system. Despite the apparent dependence of (13) on the size of the system, the L_e values are actually independent of the size L and asymptotes to a constant independent of L. Moreover, L_e provides a direct quantification of the "negative" deviations in viscosity of our blend system. The computed slip lengths L_e for the above systems for various degrees of incompatibility are plotted as a function of χN_A in Figure 6. As evident, the slip effects increase (and the apparent viscosity decreases) with an increase in the degree of incompatibility, and correspondingly the parameter L_e increases with χN. Note however that the parameter L_e for asymmetric blends embody both the velocity difference across the interface as well as the asymmetric bulk viscosities of the system. While the Figure 6 suggests that the values of L_e for asymmetric blends are comparable in magnitude to the values of L_e determined for symmetric systems, the extrapolated velocity differences across the interface (results not displayed) of an asymmetric blend (determined from Figure 5 for instance) tended to be much lower than the values determined for symmetric blends. This suggests that the slip manifests in a much less pronounced manner in asymmetric polymer blends due to the asymmetric nature of their rheological properties. Also displayed in Figure 6 are the theoretical predictions obtained by solving the integral equation of FG phenomenological theory. It is seen that while qualitatively the theoretical predictions match extremely well with our simulation results, quantitatively the theoretical predictions tend to be somewhat different than our numerical results. The latter suggests that the phenomenological constitutive equation proposed by FG[32] might need to be embellished to account for the asymmetric rheological properties of the blend components.

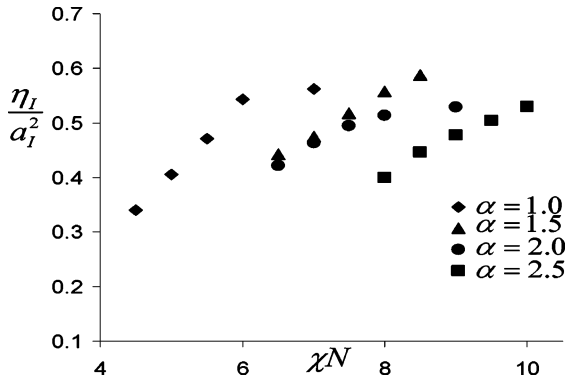

Figure 7. Interfacial viscosities η_I normalized by the square of their interfacial widths, a_I.

Next, we verify if our above results for symmetric and asymmetric blends can be collapsed onto a single curve when plotted in terms of the interfacial viscosities and the interfacial thicknesses of the blends. To do this, we solve the continuum problem with two bulk media and a single interfacial medium in between with a reduced viscosity. By fitting the velocity profile obtained in our simulations with the continuum problem, we extract η_I/η_{bulk}. Next, we compute the interfacial thickness a_I from the knowledge of the composition profiles. Explicitly, we find the composition gradient $d\phi/dx$ at the interface and compute interfacial thickness as $a_I \simeq \Delta\phi/(d\phi/dx)$. Here, $\Delta\phi$ is the difference in the compositions of the component in the two phases.

According to the scaling arguments proposed by deGennes,[42] the interfacial viscosity η_I depends only on the number of monomers in the interfacial region and hence should scale a_I^2. As mentioned earlier, the scaling predictions of deGennes is expected to be valid only at strong degrees of segregation where the interfacial width is smaller than that of the unperturbed radius of gyration of the chains. Figure 7 displays the ratio η_I/a_I^2 obtained from our simulations plotted as a function of the parameter χN in those blend components. We find that at weak segregations the value of η_I/a_I^2 is small and nonuniversal, confirming that the slip effects are negligible for partially miscible blends. In such situations, the interfacial widths are large, and the interfacial viscosity matches that of homogeneously mixed phases. However, at stronger degrees of segregation the different plots plateau to a constant value independent of the asymmetry or the degree of segregations. Our results quantitatively reinforce the scaling description of slip provided by deGennes and suggests that for unentangled interfaces the interfacial viscosity can be deduced on the basis of a thermodynamic approach by

correlating it to the interfacial width. These results also suggest that for segregated systems with small interfacial widths the interfacial viscosity can be a very small value.

As mentioned earlier, our simulations pertain to the situation involving unentangled bulk components with unentangled interfaces. Consequently, the extrapolations lengths L_e determined from our simulations are small in magnitude (of the order of a few R_g) compared to the macroscopic length scales typically encountered. In such situations, while the apparent viscosity of the blend is still lower than the bulk viscosities, the magnitude of lowering is hard to detect in experiments. On the other hand, for the more practically relevant cases of entangled bulk components with unentangled interfaces, our results for the interfacial viscosity are still applicable. In these situations, our results suggests $\eta_I \sim a_I^2$, while the bulk viscosities $\eta_B \sim N^{3-3.4}$. The apparent viscosity η_{app} can be estimated using a simple three-layer model as $\eta_{app} \sim L\eta_I/a_I \sim La_I$, and hence $L_e \sim \eta_B/a_I$ which can be very large in magnitude. These results suggest that for entangled components with unentangled interfaces the slip effects deduced from our simulations can lead to pronounced discontinuities in the velocity profiles at the interface and concomitantly to a significant lowering of the apparent viscosity of blends as seen in experiments.

In summary, our simulation results clearly display the occurrence of slip phenomena during the shear flow of polymer blends. The slip effects increase with an increase in the degree of segregation or a decrease in the interfacial thickness between the blend components. These results qualitatively agree with the experimental results of Lam and co-workers.[45] We do find that the degree of slip and its variation with the incompatibility between the components becomes less pronounced when the blends have asymmetric rheological properties. We have verified the latter result by additional simulations (not displayed) probing a wider range of asymmetry between the blend components. We also find that the phenomenological theories and scaling arguments agree remarkably well with our simulation results for both symmetric and asymmetric blends. Importantly, our simulations do confirm the scaling prediction of de-Gennes that the interfacial viscosity scales as the interfacial width of the polymer blend components for strongly segregated systems.

V. Block Copolymer Compatibilizers

It is common in many industrial applications to improve the properties of polymer blends by using trace amounts of block copolymers which promote the mixing of the blend components.[2] While the precise mechanisms by which block copolymers (commonly referred to as compatibilizers) affect the morphology of blends is still under debate, at least two dominant mechanisms have been suggested. The first mechanism purports that the copolymers affect the deformation characteristics of the blend droplets by contributing to the Marangoni stresses and/or influencing the equilibrium and dynamical characteristics of the blend interfaces, such as their interfacial tension and slip phenomena.[35,48] As evidence for this mechanism, experimental studies[49] probing the shear deformation behavior of polymer droplets have indeed confirmed significant increases in the surface areas of the deforming droplets in the presence of copolymeric compatibilizers. The second mechanism proposes that the copolymers suppress coalescence and coarsening of the droplets and hence affect the morphologies of blending. The latter was physically rationalized by Sundararaj and Macosko[50] as arising from the steric repulsion of the copolymer layers upon close approach of the droplets. Milner and Xi,[35] on the other hand, proposed that the suppression of coalescence was due to a suppression of drainage arising from the Marangoni stresses at the interface. Milner and Xi's theory is purely dynamical in nature and is supported by recent experiments by Leal and co-workers,[34] who demonstrated that in the presence of block copolymers the drainage times can be enhanced by up to an order of magnitude.

While a full scale simulation of droplet coalescence and coarsening processes would enable a resolution of the above issues, such an effort is still computationally expensive. In the following, we use the molecular perspective that can be gleaned from the self-consistent Brownian dynamics approach to probe the role of block copolymer compatibilizers in modifying the dynamical properties of the polymer blend interfaces. We focus on two main issues:

(a) The suppression of slip by block copolymers: Many recent experiments which have probed the rheology (the viscosity) of polymer blends containing block copolymeric additives have demonstrated concomitant increases in the viscosities in compatibilized blends. For instance, Zhao and Macosko[44] measured the shear viscosities for compatiblized and incompatibilities phase-separated PP and PS blend and showed that, with the addition of block copolymer compatibilizers, the negative deviations of viscosities of blends (the signature of slip phenomena) were reduced considerably. Block copolymers are believed to effect a suppression of slip by increasing the number of entanglements at the interface. However, very few studies have systematically examined the role of different controlling parameters such as the volume fraction, molecular weight of the block copolymers, etc., in modifying the slip characteristics. Our studies probe whether indeed block copolymers suppress the slip at polymer blend interfaces and the role of the amount of compatibilizer added and the block copolymer molecular weight in influencing these characteristics.

(b) Dynamics of compatibilized polymer blend interfaces: We also study the dynamics of polymer blend interfaces at compatibilizer coverages higher than that required for the suppression of slip. The main motivation for these studies is toward the resolution of mechanisms by which block copolymers suppress coalescence. While the Milner−Xi hypothesis postulating the dynamical inhibition of drainage seems consistent with many experimental results, unresolved issues still linger. For instance, their theory predicts that the critical copolymer concentrations required to prevent coalescence should increase linearly with the applied shear rate. However, experiments[51] show that there was only either a weak or absolutely no dependence between the critical concentration and the shear rate. Other experimental results have suggested that suppression was pronounced in cases where longer copolymers were dangling from the droplet surface into the continuous matrix phase. Such dependencies cannot be explained by dynamical theories and suggest that, unlike small molecule surfactants, the thickness of the copolymer layer could have a nontrivial effect in suppressing coalescence.

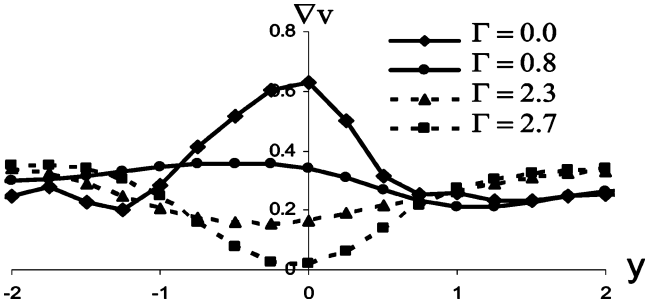

Figure 8. Velocity gradient profiles near the interface in the presence of block copolymeric compatibilizers for different coverages Γ of block copolymers. Γ is expressed as number of chains per R_g^2 of the block copolymer. The average shear rate in the bulk is 0.3 and is indicated as a dashed line in the plot. The profiles have been plotted only in the region close to the interfacial region.

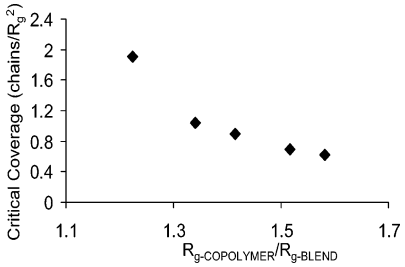

Figure 9. Molecular weight dependence of the minimum coverage of block copolymers needed to suppress slip. The molecular weights of the blend components are kept a constant at 20 beads each.

A. Results. We begin our simulations for a symmetric phase-separated blend ($A + B$) by explicitly positioning all the block copolymers (AB) at the interface. The system is then allowed to equilibrate until the composition profiles of the homopolymer and the copolymer converge. To ensure that the system has equilibrated, we checked the resulting equilibrium composition profiles against the predictions of self-consistent-field theory. Homogeneous shear is then applied using the Lee−Edwards[46] boundary condition, and the self-consistent velocity profiles were obtained for a compatibilized polymer blend for various volume fractions and molecular weights of copolymers.

To display the dynamical effects of block copolymers, we first focus on the qualitative characteristics of the gradients of the self-consistent velocities (i.e., the local shear rates) as a function of the block copolymer coverage at the interface (Figure 8). In this context, slip is manifested as a reduction in viscosity or a corresponding increase in the observed shear rate. As is evident from the displayed results, for trace or no amount of copolymers at the interface, the qualitative characteristics of the velocity profile is unchanged from that of the pure blend, displaying slip at the interface. On the other hand, for slightly higher volume fractions copolymers (corresponding to a coverage of 0.78 copolymers/R_g^2, which is still lower than the typical experimental values), our results manifest the slip suppressing feature of block copolymer. At this coverage, the local shear rates acquire an almost uniform value throughout the bulk and interface. Upon further increase in the coverage of the block copolymer, the velocity profiles display two dynamically distinct interfacial regions. The first region is near $x = 0$ (interface) and corresponds to an increased viscosity layer arising from the block copolymers, while the second layer is the slip layer at the block copolymer−matrix interfaces. At even these low values of the block copolymer concentration, the slip at the polymer blend interface has been completely suppressed. An even further increase in the volume fraction of the copolymer eliminates slip in its entirety, leaving just a single increased viscosity layer at the interface.

Our results above suggests that the copolymer layer suppresses the slip by providing an additional mechanism of friction. Note that all our above results were obtained for a Rouse system of chains where entanglements are absent. Further, all the volume fractions involved here are less than or equal to that used in experimental studies of droplet deformation in the presence of a compatibilizer. For instance, the highest coverage of copolymer (Figure 8) is 2.73 copolymers/R_g^2. The main conclusions we draw from the above results is that even small fractions of copolymer can counterbalance the slip present in polymer blends. Moreover, while entanglements probably affect the quantitative details of this suppression, entanglement with the compatibilizers is not an essential ingredient for suppressing slip.

We investigate quantitatively the role of the different features of the compatibilizers by first probing the role of the molecular weight of the block copolymer in influencing the coverages required to completely suppress the slip. Figure 9 plots the critical interfacial coverage (normalized as number of chains per R_g^2) as a function of the molecular weight of the copolymer. We deduce this critical volume fraction by determining the coverage at which the average velocity gradient across the interface matches the velocity gradient in the bulk. As is evident from the plot, the minimum coverage of the block copolymer decreases with increasing molecular weight, and for the highest MWs of copolymers considered coverages as low as 0.6 chains/R_g^2 suffice to suppress slip. The dependence of this minimum coverage on the MW can be understood as a result of the increase in the number of monomers of the blend components present in the volume spanned by the block copolymer chains at the interface. In the unentangled polymers we consider, the friction due to the copolymer layer is expected to scale as the number of monomers spanning the copolymer layer. Consequently, higher molecular weights of copolymer lead to an enhanced friction effect, which leads to a corresponding decrease in the coverage needed for suppression of slip.

We next consider the regime where the volume fractions of block copolymers, albeit low, are higher than the minimum coverages required to suppress slip. This regime corresponds to the situations where the copolymers have been reported to suppress coalescence. Our results presented in Figure 8 suggested that in this regime the copolymers qualitatively act as a layer of additional friction for the flow of blend components. These effects are displayed in Figure 10, where we illustrate explicitly the changes in the steady-state velocity profiles of compatibilized blends with changing MW and the coverages of the copolymers. The profiles displayed suggest that even at such low coverages, copolymers act to suppress the flow in the layer occupied by the copolymers. Moreover, Figure 10b suggests that an increase in MW of the copolymer increases the effective thickness of the friction layer, while a decrease in coverage (with fixed MW) leads to (Figure 10c) a decrease in the effective friction itself. To quantify these

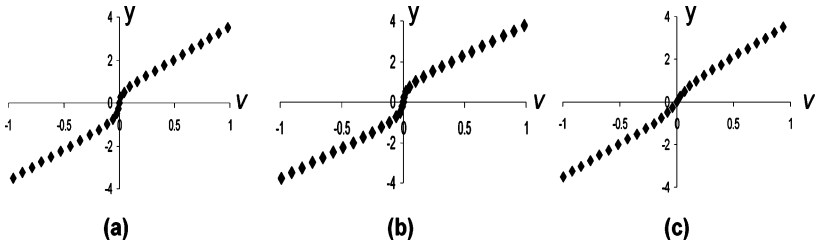

Figure 10. Velocity profiles in the presence of the compatibilizer for coverages higher than the minimum coverage required for suppression of slip. Plot (a) corresponds to a coverage $\Gamma = 3.2$ and $N_{AB} = 30$; (b) $\Gamma = 2.3$ and $N_{AB} = 40$; (c) $\Gamma = 2.7$ and $N_{AB} = 30$.

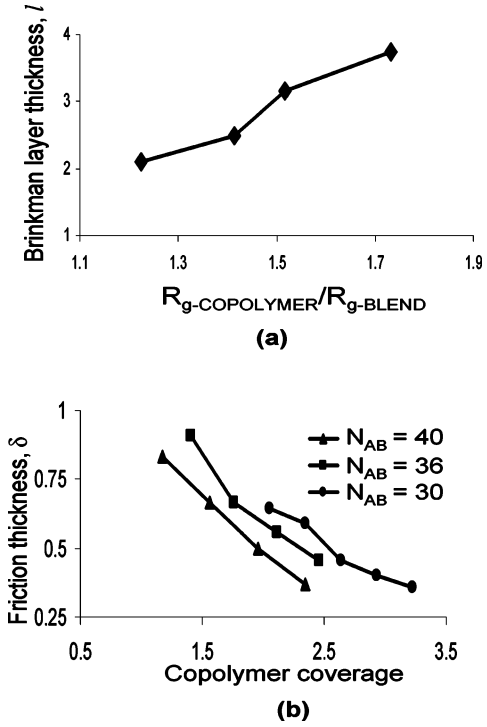

Figure 11. (a) Brinkman layer thickness, l, as a function of the copolymer lengths. (b) Brinkman friction thickness δ (see Appendix) plotted for three different molecular weights of copolymer as a function of the copolymer coverages at the interface (expressed as number of chains/R_g^2). Lines are drawn as a guide to the eye.

dynamical effects and the mutual interplay between the roles of the coverage and the molecular weight, we model the copolymer layer as a Brinkman medium.[52,53] As explained in the Appendix, there are two different length scales in the Brinkman model, namely, the Brinkman layer thickness l (representing the thickness of the friction layer) and the Brinkman friction thickness δ (representing the effectiveness of copolymers in suppressing flow). We extract these parameters from our Brownian dynamics simulations by fitting it with the analytically obtained shear velocity profile of the Brinkman model (see Appendix). Below, we discuss the effect of the MW and coverage upon the parameters of Brinkman model.

The Brinkman layer thickness extracted by fitting our simulation results is plotted in Figure 11a for four different values of the block copolymer lengths. Note that the length of the blend components are held a constant at 20 segments, while the MW of the block copolymer is varied. In accord with the qualitative results presented earlier, the Brinkman layer thickness increases with the length of the dangling copolymer, suggesting that copolymers with longer arms dangling in the matrix present a thicker region for the suppression of flow. This thickness can be simply understood as corresponding to the thickness of the block copolymers swollen by the respective blend components (note that R_g in the figures correspond to unperturbed radius of gyration of the blend components). At these extremely low coverages, an increase in the coverage of the block copolymer (results not displayed) showed no significant impact upon the Brinkman layer thickness. We note that for higher coverages the latter is not expected to be true, especially as one reaches the interfacial coverages representative of the polymer brush regime. It is interesting to note that the thickness of the layer is of the order of R_g of the copolymer. For typical polymeric blends, this is of the order of a few nanometers and is comparable to the size scales of the gap between the polymer droplets during drainage prior to coalescence. We explore the significance of these length scales in the next section.

Figure 11b displays the Brinkman friction thickness δ (expressed in units of R_g of the blend components) as a function of copolymer coverages and for different copolymer MWs. Physically, the friction thickness corresponds to the penetration thickness of the flow into the copolymer layer. As is evident from the results, even at these low coverages, the values of δ are all less than one, suggesting that the flow does not penetrate beyond a fraction of the R_g of the copolymers. Further, the penetration depth decreases almost linearly (at these coverages) with an increase in the coverage of the copolymer. While many earlier researches have studied the penetration of flow into brushes, our results suggest that significant suppression of flow can result even at very low fractions of compatibilizers. The latter feature contrasts with the density profiles of the different components at such low coverages (not displayed) which shows a significant mixing between the blend components and the respective blocks of the copolymer. These results serve to underline the importance of the molecular configurations and the resulting nonlocal coupling between density and the velocity profiles.

In Figure 11b, we have also displayed our results corresponding to the effect of the MW of the copolymer in influencing these friction characteristics. As is evident, longer copolymers provide more effective friction (at the same coverages, as expressed in number of chains/R_g^2 of the copolymer) in suppressing the flow of the blend components. This result is not surprising when viewed in the context of our results for the minimum coverages required for the suppression of slip, where we argued that the effective friction is due to the number of monomers of the blend components spanning the block copolymer layer and that this quantity increases with MW of the copolymer. However, it is to be noted that this result is somewhat dependent on our idealization of the copolymer layer as a brush with uniform friction coefficient and might lead to qualita-

tively different results if an alternate/more detailed model of the copolymer layer is used.

In summary, our results presented above suggests a unique role for the block copolymers in modulating the dynamical properties of polymer blend interfaces even at extremely low volume fractions. At low coverages of the copolymer, our results confirm that the block copolymers suppress slip, albeit even in the absence of entanglements. Upon even a slight increase in copolymer fractions we have demonstrated that the compatibilizers provide an additional source of friction on a layer of thickness of the order of the R_g of the copolymer. The effective friction of the layer is sufficient to suppress the penetration of the flow to less than a fraction of the R_g of the blend components. An increase in the coverage of the copolymer serves to increase the effective friction of the layer, while it has no effect on the thickness of the friction layer. While the above results are specific to unentangled systems, we expect the results to be qualitatively valid even for entangled systems albeit with much more pronounced magnitudes for the friction effects.

B. Compatibilizer Effects on Drainage Times. As already briefly indicated, the length scales of the copolymer friction layer are comparable to the length scales encountered during drainage and coalescence. Moreover, the resulting suppression in flow can effectively increase the lubrication force between approaching droplets leading to an increase in the drainage times. In this section, we use the values of the Brinkman parameters discerned in the previous section to quantify if indeed these can lead to enhancement in drainage times comparable to those observed in experiments. To this effect, we developed a simple model of the squeeze flow between two fluid interfaces with Brinkman layers adjoining their interface. This physically corresponds to a scenario where the two droplets approaching each other are flattened under the action of capillary forces (Appendix). Our drainage model only accounts for the effect of enhanced friction owing to the copolymers. A more realistic model of the coalescence process would necessarily have to incorporate a combination of other important effects[54] like the Marangoni stresses and steric repulsion effects which are not considered in the present model and are beyond the scope of this article.

Using the Brinkman model, we derived the equations governing the drainage times of compatibilized and uncompatibilized droplets. The values of parameters appearing in the Brinkman model were chosen from the results of our numerical simulations. The rest of the parameters in our model are chosen in accordance with the previous investigations of Leal and co-workers.[34] The capillary numbers were chosen in the range $Ca \simeq 10^{-3}-10^{-1}$. The drainage times are computed by integrating the drainage eq 18. The experimental definition for the beginning of the drainage process is when $h \sim 0.1\ \mu$m ($\simeq$25 in units of R_g), while the minimum value of h in the fluid drainage process, i.e., when the film ruptures, was fixed at $\sim$10 nm ($\simeq$3−4 in units of R_g) (obtained by assuming that the film rupture begins at a proximity when the predominant driving for coalescence is the van der Waals attraction). We have fixed the ratio of droplet and the matrix fluid viscosities $\mu_d/\mu_m = \lambda = 1$.

With the above set of parameters we compute the (nondimensionalized) drainage times for the compatibilized blend (with Brinkman medium) and uncompatibilized blend. Figure 12a,b plots the drainage times as a function of capillary numbers for different coverages (at a fixed molecular weight) of the copolymers and for different lengths of the exterior copolymer block (at a fixed coverage). The differences in the physical characteristics of the copolymer layer translates into differences in the parameters of the Brinkman model and impacts on the drainage times. As is evident from the displayed results, the presence of the compatibilizers increases the drainage times by orders of magnitude (i.e., it takes much longer for the droplets to coalesce), especially at higher capillary numbers. This suggests that the copolymer layers can serve as effective drainage and coalescence suppressors even at very low volume fractions. Furthermore, our results in Figure 12a also suggest that while an increase in coverage leads to an increased efficiency in suppression of coalescence, these increases saturate at low volume fractions of compatibilizers. These effects may serve to explain the experimental results of Hudson et al.[55] as well as Lyu et al.[51] which showed that the addition of block copolymers beyond a certain value did not impact upon the droplet size distributions of the blend. Moreover, Figure 12b confirms that copolymers with the longer block in the matrix serve as more effective coalescence suppressors.

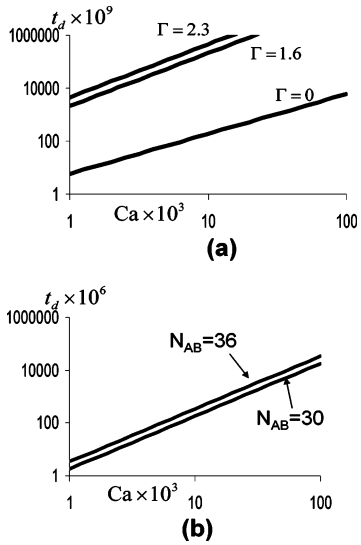

Figure 12. Nondimensionalized drainage times (t_d) plotted as a function of capillary number (Ca): (a) For three different copolymer coverages Γ (expressed as number of chains per R_g^2 at the interface. $\Gamma = 0$ corresponds to the absence of compatibilizer. (b) For two different molecular weight of copolymer, N_{AB}.

The above results are broadly consistent with the experimental results of the Leal, Macoscko, and coworkers mentioned in the Introduction. Our model is purely dynamical and does not rely upon the steric repulsion between the block copolymers. In this regard, our model rationalizes suppression as arising from the suppression of drainage of the fluid. On the other hand, by including the Brinkman parameters, our model accounts for the finite size effects of the block copolymers, which were absent in the studies which made analogies to surfactants. However, our model clearly overestimates the suppression due to compatibilizers. Indeed, while the earlier models of Marangoni stress driven suppression effectively corresponds to a compressible copolymer layer with an infinite friction between the blend and the copolymers, our model

corresponds to an incompressible copolymer layer with a finite friction between the blend and copolymers. In reality, the copolymers influence suppression in both ways, viz., by providing an additional layer of friction for drainage as well as through the Marangoni effects.[35] This combination, especially through the friction provided by an inhomogeneous copolymer layer, might possibly rationalize quantitatively the experimental results. Our main contribution in this section is to point out the possible impact of the friction effects by using the parameters and insights determined from our self-consistent Brownian dynamics simulations.

VI. Summary

In this article we used the recently proposed Brownian dynamics simulation[30] approach to study the dynamics of inhomogeneous polymeric systems. In this coarse-grained hybrid approach, the statistics of single chain in an external potential is used to account for the interactions between different chains. This considerably reduces the computational expense and enables us to study denser systems and access longer length and time scales and hence helps us perform numerical studies in parameter ranges or situations where approximate analytical tools are either inadequate or fail. Furthermore, experimental studies of polymeric systems are often interpreted in terms of parameters (e.g., Flory parameter χ) and predictions derived from the field theory models which form the basis of our method. As a consequence, it is very straightforward to connect experimental data with results from our simulations.

In the context of polymer blends, we have studied binary systems of symmetric and asymmetric polymers. We demonstrated the success of our hybrid approach in capturing the equilibrium properties of both these systems. We applied our approach to study the effect of compositional inhomogeneity on the dynamics of of such systems. Slip phenomena at the interface of polymer blends were captured and compared with scaling results of deGennes and theoretical results of FG. Our results were obtained in the contexts of both symmetric and asymmetric systems. Quantitative agreement of the extrapolation length (or slip length) with the theoretical results was observed.

On the role of block copolymers compatibilizers, we have demonstrated that the copolymers reduce the slip at the interface of a polymer blend. The minimum coverages required to eliminate slip at the interface was found to decrease with increasing length of the copolymer, suggesting that the finite size of copolymers play an important role in modifying the dynamical interfacial properties of a polymer blend. Moreover, we observed that low coverages of copolymer (more than that required to eliminate slip) could also provide an apparent layer of increased viscosity at the interface. We modeled this layer as a Brinkman friction layer and extracted the parameters appearing in the model using our numerical results. We observed order of magnitude differences in the drainage times (for two approaching droplets) of compatibilized and free droplets, suggesting that enhanced friction is a potential mechanism that could suppress droplet coalescence in compatibilized blends.

In a variety of other numerical simulations like molecular dynamics (MD), Brownian dynamics (BD), Monte Carlo (MC), etc., a pair potential (like LJ potential)[56] is employed. This renders the algorithm computationally intensive to study systems at realistic densities and especially inhomogeneous systems that exhibit nanoscale or macroscale phase separation. Moreover, simulating complex flow situations prove difficult and to our knowledge have never been attempted. Relatively newer methods such as dissipative particle dynamics (DPD), that use artificially soft-core repulsive potentials to model interactions between different beads, speed up the simulations by an order or magnitude.[57] This, however, leads to high fluid phase compressibilities, high fluctuation effects, and often a loss of connection to the chemical details of the underlying complex fluid. In contrast, the method used in this article seems to be relatively free of such artifacts and yields dynamical results not obtainable in a straightforward manner by other theoretical approaches. In the future, we plan to apply our method to study issues which more closely embody the interplay between the thermodynamical and rheological aspects, such as the shear-induced order−disorder transitions in polymer blends, shear-induced orientations of block copolymers, etc. Moreover, we are also currently working on extending the simulation approach to mimic entanglement effects and the resulting reptation motion of the chains. Such a development would allow us to address the issue of dynamics of entangled systems in inhomogeneous situations.

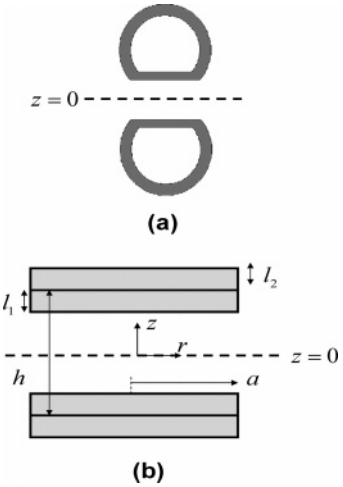

Figure 13. Schematics of the hydrodynamic model. (a) Drainage between droplets. The droplets are assumed to be flattened due to the capillary forces. (b) Closer view of the drainage between droplets. l_1 and l_2 respectively represent the thickness of the Brinkman layers exterior and interior to the droplet.

Acknowledgment. This work was partially supported by National Science Foundation under Award DMR-02-04199. We thank Profs. Glenn Fredrickson, Scott Milner, Ron Larson, and Sachin Velankar for useful discussions.

Appendix. Squeeze Flow and Drainage Time for Brinkman Medium

In this section we briefly describe the Brinkman model and derive the drainage time for two droplets with compatibilizer Brinkman layers approaching each other (see Figure 13).[52,53] The Brinkman media is characterized by two length scales: (i) The first is purely geometric (denoted as l_1 and l_2 in the figure) and represents the thickness of the layer. (ii) To mimic the enhanced friction effect of the Brinkman media, the continuum hydrodynamic equations in the Brinkman

layer are augmented with a term ξu, where ξ represents the friction of the Brinkman layer and u represents the velocity of the solvent relative to the Brinkman layer. The ratio $\delta = \xi/\mu$, where μ represents the viscosity of the solvent, has the dimensions of length and represents an effective friction length quantifying the depth of penetration of the flow.

To deduce the drainage time during droplet coalescence, in the present model we consider the scenario where the droplets are flattened (to a radius a) under the action of the capillary forces. Because of symmetry, it suffices to consider the half-plane $z > 0$. The equations governing the radial velocity field $u(z)$ in the gap between the two droplets are given by

$$\mu_m \frac{d^2u}{dz^2} - \frac{dp}{dr} = \begin{cases} 0, & 0 < z < h/2 - l_m \\ \xi u, & h/2 - l_m < z < h/2 \end{cases} \quad (14)$$

and inside the droplet phase

$$\mu_d \frac{d^2u}{dz^2} = \begin{cases} \xi u, & h/2 < z < h/2 + l_d \\ 0, & z > h/2 + l_d \end{cases} \quad (15)$$

In the above equation, μ_m represents the viscosity of the matrix and μ_d the viscosity of the droplet. l_m and l_d represent the Brinkman layer thicknesses of the compatibilizer in the matrix and the droplet phases. dp/dr denotes the pressure gradient in the gap between the approaching droplets. In the situation where the droplets are flattened by the capillary forces (to a radius a), we assume that the pressure gradient in the gap between the droplets is due to capillary forces and use a scaling approximation to replace dp/dr by $2\sigma/a^2$, where σ represents the surface tension of the drop. ξ denotes the effective friction of the Brinkman layer, which for simplicity is assumed to be the same in the droplet and the matrix phases (in the notation of the text $\delta = \sqrt{\mu_m/\xi}$). The above governing equations are supplemented by conditions ensuring continuity of the velocity fields and its derivatives and by the following boundary conditions:

$$\frac{du}{dz} = 0 \quad \text{at } z = 0 \quad (16)$$

representing the symmetry about the plane $z = 0$ and

$$\frac{du}{dz} = -\frac{u}{a} \quad \text{at } z = h/2 + l_d \quad (17)$$

In writing the latter boundary condition at the droplet interface, we have used the Chesters's scaling idea[58] that the velocity gradient inside the drop can be approximated as the velocity scale variations over a distance a.

The solution for the Brinkman problem can be combined with the lubrication theory to obtain a modified equation governing the drainage of the fluid from the gap between the droplets. In such a situation, the drainage of the fluid is obtained as

$$\pi a^2 \frac{dh}{dt} = -2\pi a \int_{-h/2}^{h/2} dz\, u(z) \quad (18)$$

We solve eqs 14−17 analytically and combine the result with a numerical solution of eq 18. The latter is performed between the limits of $h_{beg} = 0.1$ μm, corresponding to the start of the drainage, to $h_{end} \sim 10-15$ nm. The qualitative trends discussed in the main text do not depend sensitively on the exact limits we choose for the beginning and the end of drainage.

References and Notes

(1) Paul, D. R.; Bucknall, C. B. *Polymer Blends*; Wiley: New York, 2000.
(2) Macosko, C. W. *Macromol. Symp.* **2000**, *149*, 171.
(3) Lyu, S. P.; Bates, F. S.; Macosko, C. W. *AIChE J.* **2002**, *48*, 7.
(4) Chen, Z. R.; Kornfield, J. A. *Polymer* **1998**, *39*, 4679.
(5) Hamley, I. W. *J. Phys.: Condens. Matter* **2001**, *13*, R643.
(6) Tepe, T.; Hajduk, D. A.; Hillmyer, M. A.; Weimann, P. A.; Tirrell, M.; Bates, F. S.; Almdal, K.; Mortensen, K. *J. Rheol.* **1997**, *41*, 1147.
(7) Wiesner, U. *Macromol. Chem. Phys.* **1997**, *11*, 3319.
(8) Vigild, M. E.; et al. *Macromolecules* **2001**, *34*, 951.
(9) Fernandez, M. L.; Higgins, J. S.; Richardson, S. M. *J. Mater. Proc. Technol.* **1996**, *56*, 807.
(10) Hindawi, I. A.; Higgins, J. S.; Weiss, R. A. *Polymer* **1992**, *33*, 2522.
(11) Soontaranun, W.; Higgins, J. S.; Papathanasiou, T. D. *Fluid Phase Equilib.* **1996**, *121*, 273.
(12) Bates, F. S.; et al. *Macromolecules* **2002**, *35*, 4685.
(13) Bird, R. B.; Curtiss, C. F.; Armstrong, R. C.; Hassager, O. *Dynamics of Polymeric Liquids*; Wiley: New York, 1987; Vol. 2.
(14) Doi, M.; Edwards, S. F. *The Theory of Polymer Dynamics;* Oxford University Press: Oxford, 1986.
(15) Matsen, M. W.; Schick, M. *Phys. Rev. Lett.* **1994**, *72*, 2660.
(16) Fraaije, J. G. E. M.; et al. *J. Chem. Phys.* **1997**, *106*, 4260.
(17) Fredrickson, G. H.; Ganesan, V.; Drolet, F. *Macromolecules* **2002**, *35*, 16.
(18) Matsen, M. W. *Phys. Rev. Lett.* **1995**, *74*, 4225. Matsen, M. W. *Macromolecules* **1995**, *28*, 5765.
(19) Matsen, M. W. *J. Chem. Phys.* **1997**, *106*, 7781. Chen, H. Y.; Fredrickson, G. H. *J. Chem. Phys.* **2002**, *116*, 1137. Horvat, A.; et al. *J. Chem. Phys.* **2004**, *120*, 1117.
(20) Ottinger, H. C. *Stochastic Processes in Polymeric Fluids;* Springer: Berlin, 1996.
(21) Masubachi, Y.; et al. *J. Chem. Phys.* **2001**, *115*, 4387.
(22) Padding, J. T.; Briels, W. J. *J. Chem. Phys.* **2002**, *117*, 925.
(23) Doi, M.; Takimoto, J. *Philos. Trans. R. Soc. London A* **2003**, *361*, 641.
(24) Jendrejack, R. M.; et al. *J. Chem. Phys.* **2004**, *120*, 2513.
(25) Fraaije, J. G. E. M. *J. Chem. Phys.* **1993**, *99*, 9202. Hasegawa, H.; Doi, M. *Macromolecules* **1997**, *30*, 3086.
(26) Maurits, N. M.; Zvelindovsky, A. V.; Fraaije, J. G. E. M.; et al. *J. Chem. Phys.* **1997**, *109*, 11032.
(27) Doi, M.; Onuki, A. *J. Phys. II* **1992**, *2*, 1631. Milner, S. T. *Phys. Rev. E* **1993**, *48*, 3674. Fredrickson, G. H. *J. Chem. Phys.* **2002**, *117*, 6810.
(28) Shima, T.; et al. *Macromolecules* **2003**, *36*, 9199.
(29) Schnidman, Y.; Gersappe, D. Personal communication.
(30) Ganesan, V.; Pryamitsyn, V. *J. Chem. Phys.* **2003**, *118*, 4345.
(31) Brochard-Wyart, F.; deGennes, P. G. *C. R. Acad. Sci., Ser. II* **1990**, *310*, 1169.
(32) Goveas, J. L.; Fredrickson, G. H. *Eur. Phys. J. B* **1998**, *2*, 79.
(33) Lodge, T. P.; Dalvi, M. C. *Phys. Rev. Lett.* **1995**, *75*, 657. Vigild, M. E.; Chu, C.; Sugiyama, M.; Chaffin, K. A.; Bates, F. S. *Macromolecules* **2001**, *34*, 951.
(34) Ha, J. W.; Yoon, Y.; Leal, L. G. *Phys. Fluids* **2003**, *15*, 849.
(35) Milner, S. T.; Xi, H. W. *J. Rheol.* **1996**, *40*, 663.
(36) Maurits, N. M.; Fraaije, J. G. E. M.; et al. *J. Chem. Phys.* **1997**, *107*, 5879.
(37) Clarke, N.; McLeish, T. C. B. *Phys. Rev. E* **1998**, *57*, R3731.
(38) Clarke, N.; McLeish, T. C. B. *Macromolecules* **1999**, *32*, 4447.
(39) Utracki, L. A.; Kamal, M. R. *Polym. Eng. Sci.* **1982**, *22*, 96. Utracki, L. A. *Polym. Eng. Sci.* **1983**, *23*, 602.
(40) Han, C. D.; Yu, T. C. *J. Appl. Polym. Sci.* **1971**, *15*, 1163. Han, C. D.; Yu, T. C. *Polym. Eng. Sci.* **1972**, *12*, 81.
(41) Utracki, L. A. *J. Rheol.* **1991**, *35*, 8.
(42) de Gennes, P. G. *C. R. Acad. Sci. Paris, Ser. B* **1979**, *288*, 219.
(43) Barsky, S.; Robbins, M. O. *Phys. Rev. E* **2001**, *63*, 021801.
(44) Zhao, R.; Macosko, C. W. *J. Rheol.* **2002**, *46*, 145.
(45) Lam, Y. C.; et al. *J. Rheol.* **2003**, *47*, 795.

(46) Allen, M. P.; Tildesley, D. J. *Computer Simulation of Liquids;* Oxford University Press: Oxford, 1987.
(47) Bousmina, M.; Palierne, J. F.; Utracki, L. A. *Polym. Eng. Sci.* **1999**, *39*, 1049.
(48) de Gennes, P. G. *C. R. Acad. Sci., Ser. II* **1989**, *308*, 1401. Brochard, F.; de Gennes, P. G.; Troian, S. *C. R. Acad. Sci., Ser. III* **1990**, *310*, 1169.
(49) Levitt, L.; Macosko, C. W. *Macromolecules* **1999**, *32*, 6270.
(50) Sundararaj, U.; Macosko, C. W. *Macromolecules* **1995**, *28*, 2647.
(51) Lyu, S.; Jones, T. D.; Bates, F. S.; Macosko, C. W. *Macromolecules* **2002**, *35*, 7845.
(52) Milner, S. T. *Macromolecules* **1991**, *24*, 3704.
(53) Fredrickson, G. H.; Pincus, P. *Langmuir* **1991**, *7*, 786.
(54) Blawzdzeiwicz, J.; Wajnryb, E.; Loewenberg, M. *J. Fluid Mech.* **1999**, *29*, 395.
(55) Hudson, S. D.; et al. *Macromolecules* **2000**, *33*, 371.
(56) Binder, K. In *Computational Modeling of Polymers*; Bicerano, J., Ed.; Springer: Berlin, 1992. Kremer, K. In *Soft and Fragile Matter: Nonequilibrium Dynamics, Metastability and Flow*; Cates, M. E., Evans, M. R., Eds.; IOP Publishing: Edinburgh, 2000.
(57) Groot, R. D.; Warren, P. B. *J. Chem. Phys.* **1997**, *107*, 4423.
(58) Chesters, A. K. *Trans. Inst. Chem.* **1991**, *69*, 259.

MA048986A